RESEARCH ARTICLE doi.org/10.1002/adsc.70007

ADVANCED SYNTHESIS & CATALYSIS

Catalyst-Directed Selectivity in Vinylcarbene Reactions: A Comparative Study of Ag, Rh, and Cu Complexes

Roger Monreal-Corona,[a] Àlex Díaz-Jiménez,[a] Pedro J. Pérez,[b] Ana Caballero,[b] Anna Roglans,[a] Albert Poater,[a,*] and Anna Pla-Quintana[a,*]

[a] Institut de Química Computacional i Catàlisi (IQCC) and Departament de Química, Universitat de Girona (UdG), Facultat de Ciències, C/ Maria Aurèlia Capmany 69, Girona 17003, Catalunya, Spain
E-mail: albert.poater@udg.edu; anna.plaq@udg.edu
[b] Laboratorio de Catálisis Homogénea, Unidad Asociada al CSIC, CIQSO-Centro de Investigación en Química Sostenible and Departamento de Química, Universidad de Huelva, Huelva 21007, Spain

Manuscript received: April 14, 2025; Revised manuscript received: June 6, 2025;
Version of record online: June 29, 2025

Supporting information for this article is available on the WWW under https://doi.org/10.1002/adsc.70007

Abstract: A comprehensive mechanistic investigation is conducted to uncover the factors governing the selectivity of Ag, Rh, and Cu catalysts in vinylcarbene-mediated reactions. The study examines the preference for carbenic versus vinylogous C(sp^3)─H bond insertion, highlighting the critical roles of the electronic and steric properties of transition metal catalysts. Contrary to previous assumptions that the enhanced electrophilic character of the vinylogous position in metal vinyl carbenes is the primary determinant, the findings demonstrate that the stereoelectronic effects of the ligand play a more dominant role. These insights inform the design of catalytic systems with tailored selectivity, advancing predictive catalysis and C─H bond functionalization.

Keywords: alkynes, carbenes, carbenic reactivity, C─H functionalization, density functional theory, vinylogous reactivity

1. Introduction

Transition metal carbene complexes serve as highly adaptable intermediates in organic synthesis, facilitating crucial transformations. Notably, carbene transfer reactions to C─H bonds,[1] including the regio- and enantioselective modification of the relatively inert C─H bonds in alkanes,[2] have significantly advanced methods for C─C bond formation. A compelling subclass of metal carbene complexes are those containing vinylcarbenes. The conjugation between the double bond and the carbenic position not only enables [3+n]-cycloadditions[3] but also imparts reactivity at the vinylogous site (**Scheme 1**A). These unique features have been leveraged to develop synthetically valuable transformations, building on the foundational work of the Davies group in the 1990s,[4] and the notable contributions, among others, by the Doyle group.[5]

The selectivity in reactions involving metal–vinylcarbenes is strongly influenced by the substrate structure, and more significantly, by the choice of the metal catalyst.[6] However, only a limited number of examples have demonstrated vinylogous site insertion with activated C(sp^2)─H bonds under rhodium catalysis[7] or with various X─H bonds (X = O, N, and F) using different metals.[8] As a general trend, reactions mediated by rhodium vinylcarbene intermediates—accounting for the majority of reported cases—exhibit typical carbene reactivity, albeit with some notable exceptions.[7] In contrast, coinage metal catalysts, which have been much less explored, predominantly target the vinylogous carbon. This difference in reactivity has primarily been attributed to the enhanced electrophilic character of the vinylogous position in coinage metals vinylcarbene intermediates.[9]

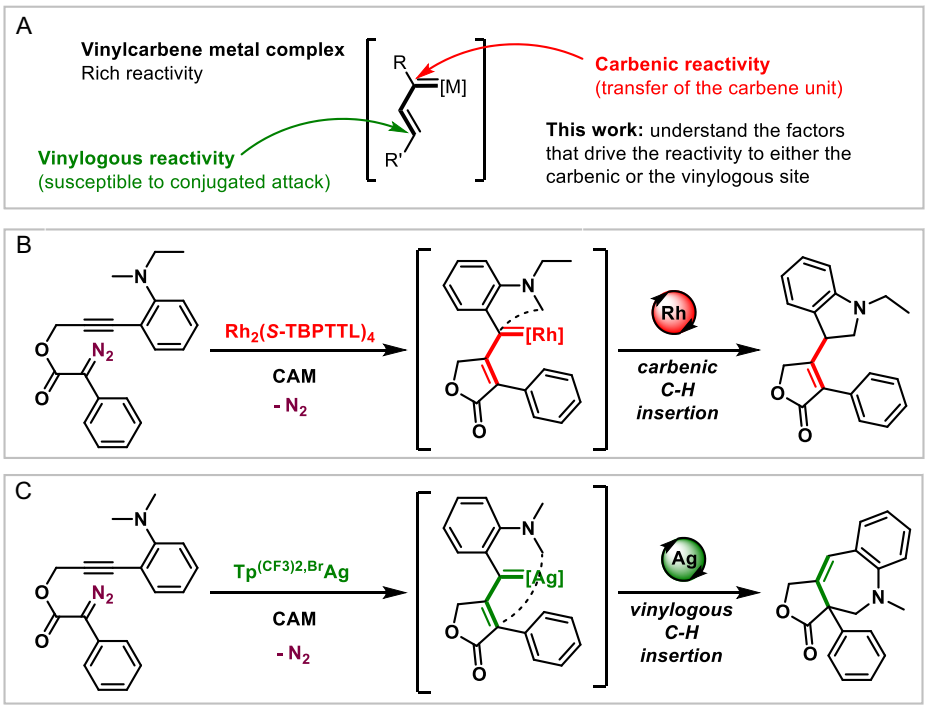

Scheme 1. The dual reactivity of vinylcarbenes. A) Vinylcarbene metal complex rich reactivity. B) Rh-catalyzed selective carbenic C—H insertion (Doyle and Xu). C) Ag-catalyzed selective vinylogous C—H insertion (previous results from our group).

The most straightforward method for generating vinylcarbene transition metal complexes involves the transition metal-catalyzed decomposition of vinyldiazoacetates or related arylsulfonylhydrazones.[10] However, while methods for synthesizing vinyldiazo compounds appear broadly applicable, each comes with significant limitations, particularly in terms of substrate scope. Alternative strategies have been developed to access topologically distinct vinylcarbene–metal complexes, including the electrophilic ring opening of cyclopropenes,[11] the oxidative diyne cyclizations,[12] the decarbenation via a retro-Büchner reaction of 7-substituted-1,3,5-cycloheptatrienes,[13] the gem-hydrogenation of enynes,[14] or the more broadly applicable carbene/alkyne metathesis (CAM).[15]

The CAM process, initially described by Padwa[16] and Hoye,[17] provides a route wherein a metal carbene complex, typically derived from a diazo precursor, interacts with an alkyne, transferring the carbene moiety to one of the alkyne carbons to form a vinylcarbene–metal complex. This approach, especially when executed in an intramolecular set-up, enables the efficient construction of polycyclic structures through CAM cascades, which can culminate in diverse carbene transformations.[18,19]

Research by Doyle and Xu[20] on chiral dihydroindole synthesis via CAM cascades with propargyl diazoacetates has shown that selective C(sp^3)—H bond insertion at the carbene site can be achieved by fine-tuning the ligands of dirhodium complexes (Scheme 1B). In contrast, our groups have recently shown that in an almost analogous substrate (replacing the ethylmethylamino group with a dimethylamino group), the use of silver tris-pyrazolylborate catalysts achieves intramolecular interception of the remote position of vinylcarbene–silver intermediates by C(sp^3)—H bond insertion granting access to azepine derivatives (Scheme 1C).[21]

In this work, we present a mixed computational and experimental study on the reactivity of Ag, Rh, and Cu with a probe substrate, aiming to elucidate the factors that direct the reactivity toward either carbenic products (CAR) or vinylogous products (VIN). Contrary to previous proposals, our findings reveal that stereoelectronic interactions between the ligand and the substrates outweigh the differences in electrophilicity of the two reactive sites of the vinylcarbene–metal intermediate.

2. Results and Discussion

The study was initiated by evaluating the reaction of the dimethylamino substrate **1** under rhodium catalysis using $Rh_2(OAc)_4$ and $Rh_2(esp)_2$, and the results were compared to those previously obtained[21] with silver (**Table 1**). $Rh_2(OAc)_4$ promoted an overall yield of 73% with a **CAR**:**VIN** ratio of 74:26, whilst $Rh_2(esp)_2$ provided a significantly higher yield of 95%, along with an increased **CAR**:**VIN** ratio of 93:7. These findings assess the hypothesis that silver favors the vinylogous reactivity compared to rhodium. However, they also reveal that the reactivity at the two sites of the

Table 1. Comparison of the selectivity of silver- and rhodium-catalyzed reactions.

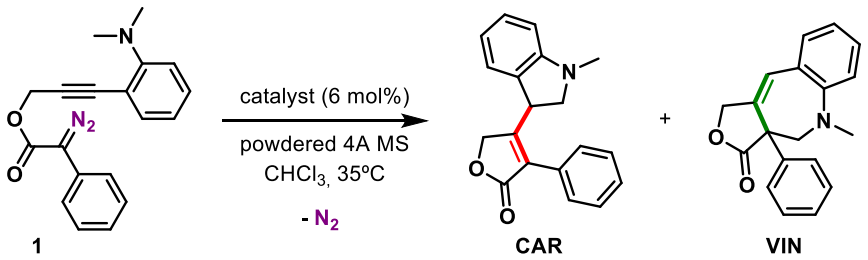

Entry[a)]	Catalyst	CAR yield [%][b)]	VIN yield [%][b)]	CAR:VIN ratio
1	$Tp^{(CF3)2,Br}Ag(THF)$	10	70	12:88
2	$[Tp^{Br3}Ag]_2$	34	35	49:51
3	$Rh_2(OAc)_4$	54	19	74:26
4	$Rh_2(esp)_2$	88	7	93:07

[a)] Reactions were carried out with 0.06 mmol of 1 ([1]=3.8 mM), at room temperature in 16 mL of $CHCl_3$ for 1.5 h;
[b)] Isolated yield.

vinylcarbene–metal intermediate is strongly influenced by the ligand coordinated to the metal. We thus turned to computational techniques (density functional theory (DFT) calculations) to investigate the mechanisms underlying the observed selectivity differences with the various catalysts. The mechanism for the silver-catalyzed transformation had already been computed,[21] and served as a reference for studying the rhodium-catalyzed reaction. The reaction was initially computed for the Rh(II) acetate dimer (see Figure S5, Supporting Information for the whole profile) and the possible pathways starting from vinylcarbene species **F** are shown in **Figure 1** (energy values depicted in gray). Initially, a hydride shift surpassing an energy barrier of 14.7 kcal mol^{-1} leads to zwitterionic intermediate **G**, which is 2.5 kcal mol^{-1} lower in energy than the preceding minimum. All attempts to locate the more conventional concerted C─H insertion from intermediate **F** in our system were unsuccessful. From **G**, the selective step determining the formation of the **CAR** and the **VIN** occurs.

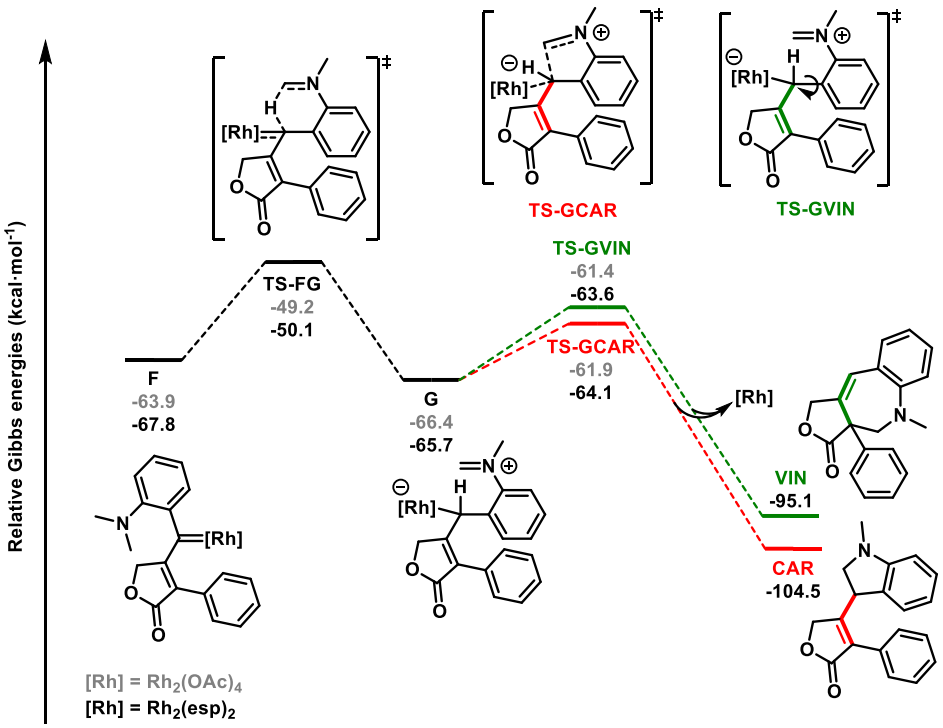

Figure 1. Reaction profile for the formation of **CAR** and **VIN** products from intermediate vinylcarbene species **F** (relative Gibbs energies in kcal mol^{-1}).

On one hand, **G** undergoes a backside S_E2[22] C─C bond-closing step to form the **CAR** via **TS-GCAR** with a kinetic cost of 4.5 kcal mol^{-1}. On the other hand, **G** can rotate and directly engage in an S_E2' reaction at the γ carbon atom, overcoming a barrier of 5.0 kcal mol^{-1} to form the vinylogous product **VIN**. The possibility of metal dissociation from intermediate **G** to generate a free carbanion prior to C─C bond formation was evaluated but found to be energetically unfavorable, and thus, ruled out. Of note, in the selectivity determining step, the iminium ion is the electrophilic fragment, and the allyl rhodium fragment is the nucleophilic one. The reaction profile was also computed for $Rh_2(esp)_2$ (Figure S5, Supporting Information and Figure 1, depicted in black), a much bulkier catalyst.

Computational results align with the experimental data, indicating that the formation of the **CAR** product is both kinetically and thermodynamically favored over the **VIN** product across the two rhodium catalysts studied. This is in contrast to the previous results with $Tp^{(CF3)2,Br}Ag$ in which the formation of the **VIN** product was kinetically but not thermodynamically favored over the formation of the **CAR** product (see Figure S1, Supporting Information). To complete the picture and evaluate the importance of the substituents on the Tp^x ligand, the reaction mechanism with the Tp^{Br3} ligand was also computed (see Figure S2, Supporting Information), resulting in the formation of the **CAR** product being both kinetically and thermodynamically favored over the formation of the **VIN** product. The computed differences in the transition state energy barriers for accessing the two products ($\Delta\Delta G^{\ddagger}$ [**TS-GVIN**–**TS-GCAR**]) are as follows: 0.5 kcal mol^{-1} for both $Rh_2(OAc)_4$ and $Rh_2(esp)_2$, 0.7 kcal mol^{-1} for $[Tp^{Br3}Ag]_2$, and −0.4 kcal mol^{-1} for $Tp^{(CF3)2,Br}Ag(THF)$. While these values generally reflect the observed trends, they do not fully account for the experimentally obtained ratios (**Figure 2**). For instance,

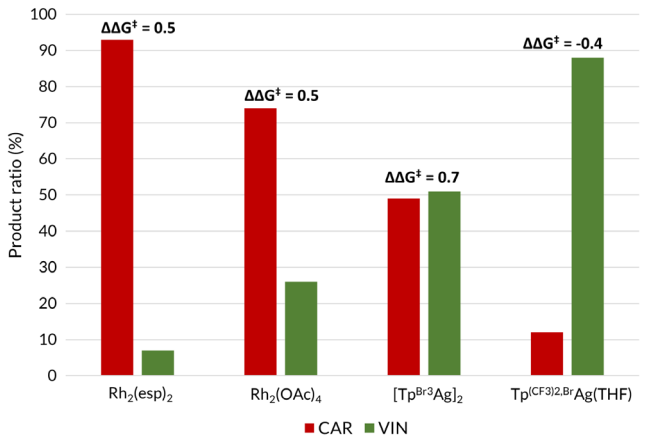

Figure 2. Product ratios (%) and computed differences in the transition state energy barriers ($\Delta\Delta G^{\ddagger}$ (**TS-GVIN**–**TS-GCAR**) in kcal mol^{-1}) for accessing the two products.

the bulkier $Rh_2(esp)_2$ catalyst results in a significantly higher **CAR**:**VIN** ratio than $Rh_2(OAc)_4$, and the models fail in predicting a higher **CAR**:**VIN** ratio for $[Tp^{Br3}Ag]_2$ than the rhodium catalysts. However, the observed differences are within the range of accuracy (1 kcal mol^{-1}), and minor errors in computed transition state energies can lead to a reversal in predicted selectivity due to the exponential relationship between activation energies and rate constants.[23] Therefore, we chose to conduct a thorough analysis of the intermediates and the transition state structures to identify steric and electronic factors that could influence the reaction selectivity.

We began by examining a series of electronic and steric descriptors to uncover potential correlations (Table S2, Supporting Information). The charge distribution analysis reveals that the carbenic carbon consistently exhibits a higher propensity for C─C bond formation. This observation suggests that the vinylogous product is unlikely to predominate in the studied systems, indicating that electronic effects, if present, play only a minor role. In contrast, analysis of the steric descriptor, specifically the buried volume (%V_{bur}),[24] reveals an opposite trend: the vinylogous position is sterically less hindered, making it more accessible for reaction. These findings suggest that more complex, multifaceted factors are influencing the observed reactivity trends.

To unravel these factors, we analyzed the 3D structures of key intermediates and transition states along the reaction pathway. Structural comparisons revealed significant geometric differences between the rhodium and the silver catalysts in the reactive forms of intermediate **G** (**Figure 3**). In the paddlewheel rhodium complexes, the planar and extended shape with minimal lateral openings and the tight coordination of the carboxylate ligands constrains the substrate into a planar-like geometry. The iminium nitrogen atom adopts an almost orthogonal orientation relative to the Rh–carbenic carbon axis (Rh─C(carbene)─N angle: 91.7°), positioning the iminium carbon closer to the carbenic carbon (2.935 Å) than to the vinylogous carbon (4.831 Å) in the rhodium vinylcarbene system. In contrast, the trispyrazolylborate ligand in the silver catalyst creates an umbrella-shaped environment with three distinct cavities and furthermore shows a labile coordination (exchanging between kappa-2 and kappa-3 along the reaction pathway).[25] In intermediate **G**, the kappa-2 coordination enlarges the available space, allowing the phenyldimethylamino group to adopt a nearly perpendicular orientation relative to the Ag–carbenic carbon axis (Ag─C(carbene) ─N angle: 175.0°). This conformation places the iminium carbon closer to the vinylogous carbon (2.553 Å) than to the carbenic carbon (3.122 Å). Notably, dispersion interactions between the aromatic ring bearing the iminium ion and the decoordinated pyrazole ring stabilize this arrangement (Figure 3C). These interactions are more pronounced in the $Tp^{(CF3)2,Br}Ag$

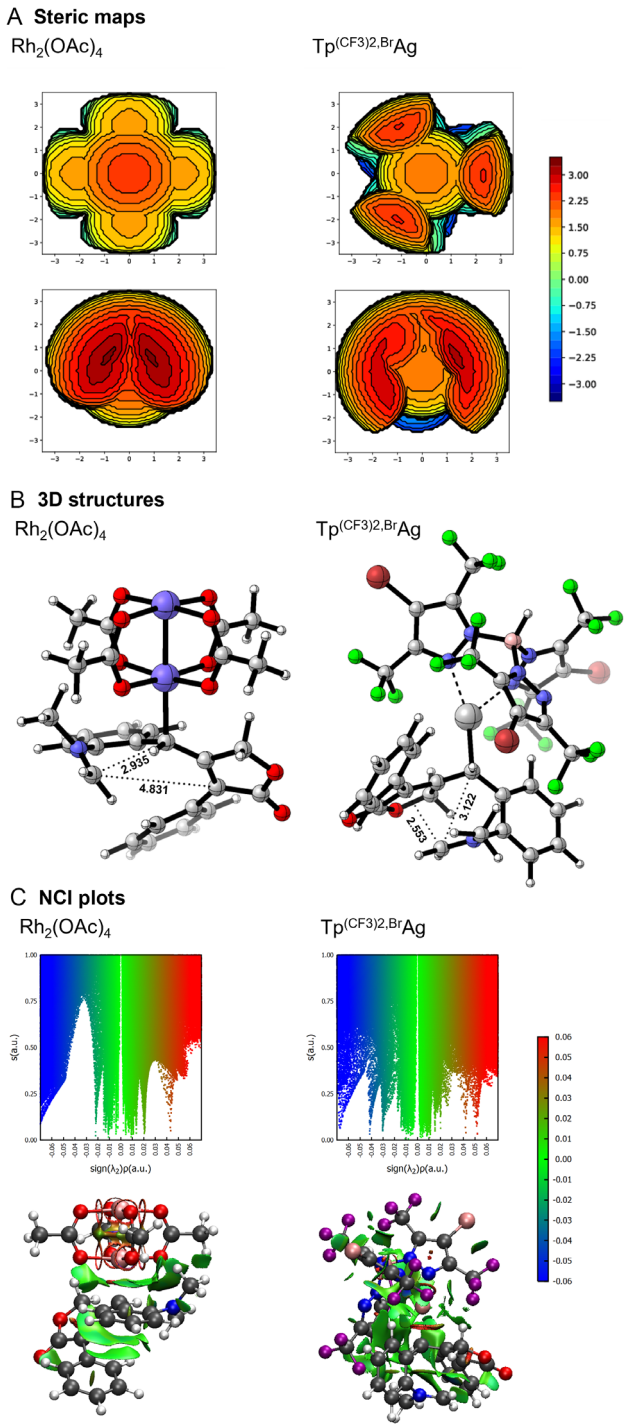

Figure 3. A) Steric maps with bottom and side view for $Rh_2(OAc)_4$ and $Tp^{(CF3)2,Br}Ag$ catalysts; B) 3D structure with selected distances between the iminium carbon, and vinylogous and carbenic sites (in Å) of species **G** for $Rh_2(OAc)_4$ and $Tp^{(CF3)2,Br}Ag$; and C) 2D and 3D noncovalent interactions plots of species **G** for $Rh_2(OAc)_4$ and $Tp^{(CF3)2,Br}Ag$ catalyst.

complex compared to the $Tp^{Br3}Ag$ complex (Figure S4, Supporting Information), correlating with the higher proportion of the vinylogous product observed for the former.

The formation of the vinylogous product in the Rh paddlewheel catalysts requires a 180° rotation of the aromatic ring attached to the iminium group (Figure 1). A dihedral angle scan revealed that no additional conformer could be located, as this rotation directly leads, in a barrierless manner, to carbon–carbon bond formation leading to the **VIN product**. Consequently, as the steric bulk of the catalyst increases, the rotation of the dihedral angle becomes increasingly hindered (compare **TS-GVIN** for $Rh_2(OAc)_4$ and $Rh_2(esp)_2$), resulting in an experimentally higher **CAR:VIN** ratio. For the silver catalysts, the iminium-substituted aromatic ring adopts a perpendicular conformation in intermediate **G**, requiring only a 90° rotation.

At this stage, it is evident that the key factors influencing reactivity at the vinylogous position are the steric bulk of the catalyst and the positioning of the phenyl ring in intermediate **G**. Both Rh and Ag catalysts yield carbenic and vinylogous products; however, the selectivity is primarily dictated by the ligand framework. The bulky paddlewheel ligands in Rh favor the **CAR**, while the umbrella-shaped environment provided by the Tp^xAg moiety promotes the vinylogous product suggesting that, to achieve selective formation of the vinylogous product, a tridentate yet labile ligand system is required.

Building on this information, we aimed to investigate the effect of altering the nature of the metal center. Copper-based catalysts are well-known for their excellent activity in carbene transfer reactions as demonstrated by their use in various cycloadditions of enoldiazocompounds.[26] Notably, copper hydrotrispyrazolylborate (Tp^xCu) complexes have been employed as catalysts in both carbene and nitrene transfer reactions.[27] Thus, Tp^xCu catalysts appeared particularly attractive for our study, as they allowed us to assess the impact of metal substitution within a well-characterized ligand platform.[28] Upon setting up the reaction with $Tp^{Br3}Cu(NCMe)$, we observed a quantitative yield for this system. However, the selectivity was notably reversed compared to our expectations, yielding a **CAR**:**VIN** ratio of 80:20 (**Scheme 2**).

The complete reaction mechanism was elucidated using DFT calculations and is shown in **Figure 4**. We initially explored a mechanistic pathway analogous to those previously reported for silver and rhodium. Similar to silver, the Tp ligand transitions from k^3-$Tp^{Br3}Cu$ to k^2-$Tp^{Br3}Cu$ coordination during the catalytic cycle.[29] Starting from the copper vinylcarbene intermediate **F**, a hydride shift with an activation barrier of 15.2 kcal mol^{-1} leads to the formation of the iminium intermediate **G**, from which kinetic barriers of 5.0 and 8.6 kcal mol^{-1} result in the formation of the **VIN** and **CAR** products, respectively. Based on these results, one would expect an almost exclusive formation of the **VIN** product, in contrast to the experimental observations. Revisiting the mechanistic pathways across different metals, we identified a notable divergence in the behavior of copper

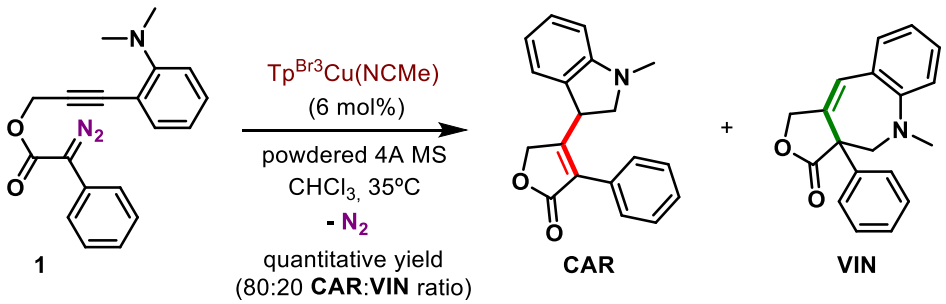

Scheme 2. $Tp^{Br3}Cu$-catalyzed CAM/C─H insertion cascade.

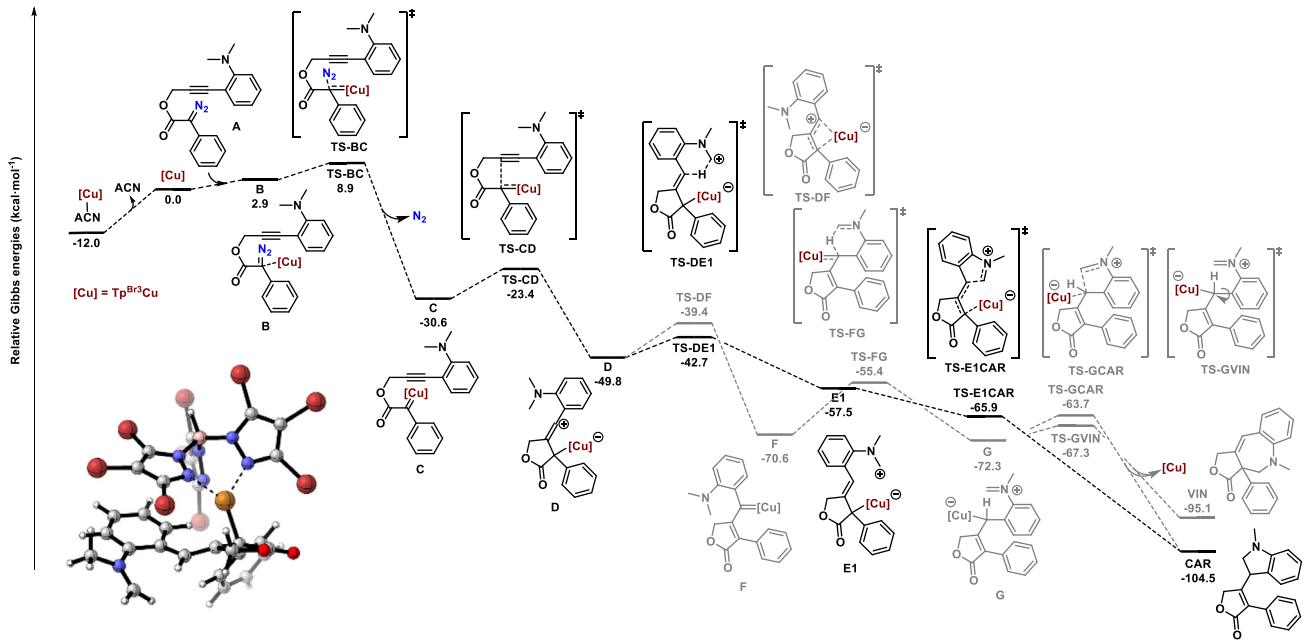

Figure 4. Gibbs energy profile (in kcal mol^{-1}) of the copper-catalyzed CAM reaction, and 3D structure of species **E1** for $Tp^{Br3}Cu$ catalyst.

and rhodium compared to silver, specifically in the formation of the metal vinylcarbene intermediate. For copper, the formation of vinylcarbene **F** from the cationic copper vinyl intermediate **D** occurs with a reaction barrier of 10.4 kcal mol^{-1}. In comparison, this step involves barriers of 13.5 and 11.0 kcal mol^{-1} for $Rh_2(OAc)_4$ and $Rh_2(esp)_2$, respectively (Figure S5, Supporting Information), while for silver, this transformation is barrierless. An alternative reactivity of vinyl cations, specifically the possibility of a hydride shift to the carbenic position, was then considered.[30] Calculations revealed that a hydride shift from the copper vinylcation **D** via transition state **TS-DE1** proceeds with an activation barrier of only 7.1 kcal mol^{-1}, leading to the zwitterionic intermediate **E1**. Notably, this barrier is 3.3 kcal mol^{-1} lower than the competing pathway involving the formation of vinylcarbene species **F**. Furthermore, **E1** evolves into the **CAR** product in a barrierless process (**TS-E1CAR**), bypassing the vinylcarbene species entirely. This new mechanistic pathway aligns with the experimental results, where the **CAR** product emerges as the major species via a route that bypasses the vinylcarbene intermediate **F**. Conversely, the pathway involving the vinylcarbene species **F** preferentially leads to the formation of the **VIN** product. The relatively high barrier for the back-conversion of **F** to **D** explains the observed mixture of **CAR** and **VIN** products. For rhodium, a distinct scenario arises. Intermediate **E1** does not progress to the **CAR** product, as no corresponding transition state could be located. Reaction coordinate scans consistently reverted to **E1**, rendering this pathway nonproductive. Lastly, in the case of silver, the hydrogen shift to the carbenic position from intermediate **D** is energetically unfavorable compared to formation of **F**, discarding this alternative pathway.

3. Conclusions

This work highlights the intricate interplay of steric and electronic factors in governing the selectivity of

C(sp^3)─H bond insertions into vinylcarbene–metal intermediates. While paddlewheel rhodium catalysts favor carbenic pathways due to steric constraints, Tp^x-silver catalysts promote vinylogous insertion through their flexible ligand environment and dispersion interactions between the trispyrazolyl arms and the substrate. In contrast, Tp^x-copper catalysts exhibit a distinct reactivity, bypassing traditional vinylcarbene intermediates in favor of **CAR product**s via a pathway involving a vinyl cation. Beyond mechanistic insights, this study contributes to predictive catalysis[31] by providing a framework for accelerating catalyst design and emphasizing the complexity of reaction selectivity. It underscores the importance of evaluating multiple reaction pathways, particularly in transition metal-catalyzed processes, where the interplay of electronic and steric factors plays a critical role. These findings not only advance our understanding of transition metal catalysis but also guide the development of selective methodologies for complex C─H bond functionalizations. Future studies integrating predictive catalysis tools will further refine these methodologies, enhancing their efficiency and applicability across diverse substrates.

4. Computational Details

All geometry optimizations and analytical vibrational frequency calculations were carried out using the Gaussian16 software package (revision A.03).[32] The BP86 functional developed by Becke and Perdew was used,[33] together with the Grimme D3 correction term for the electronic energy.[34,35] The electronic configuration of the molecular systems was described with the SDD basis set and pseudopotentials for Ag and Cu,[36] the LANL2DZ basis set containing effective core relativistic pseudopotentials for Rh,[37] and the Def2-SVP basis set with polarization functions of Ahlrichs and coworkers for the rest of atoms.[38] The intrinsic reaction coordinate procedure was used to confirm the two minima connected by each transition state.[39] To improve accuracy, single point energy calculations were carried out with the B3LYP hybrid exchange–correlation functional,[40] and the Def2-TZVP for nonmetal atoms.[41] Moreover, solvent effect corrections were included to simulate a dichloromethane solution by means of the universal solvation model SMD of Cramer and Truhlar.[42] As a summary, the reported Gibbs energies are obtained at the B3LYP-D3/Def2-TZVP-LANL2DZ(Rh)-SDD(Ag and Cu)-SMD(DCM)//BP86-D3/Def2-SVP-LANL2DZ(Rh)-SDD(Ag and Cu) level of theory together with gas-phase thermal and entropic contributions computed at 298 K and 1 atm at the BP86-D3/Def2-SVP-LANL2DZ(Rh)-SDD(Ag and Cu) level of theory.

Acknowledgements

The authors are grateful for financial support from the Ministerio de Ciencia e Innovación (PID2021-127423NB-I00, PID2023-146946NB-I00, and PID2023-146849NB-I00/MICIU/AEI/10.13039/501100011033/FEDER, UE projects, and the OASIS Network RED2022-134074-T) and the Generalitat de Catalunya (Project no. 2021-SGR-623). The authors thank the Spanish Ministerio de Universidades for pre-doctoral fellowships FPU20/00707 to R.M.-C. and FPU2018/02912 to À.D.-J. A.P.Q. and A.P. are Serra Húnter Fellows.

Conflict of Interest

The authors declare no conflict of interest.

Data Availability Statement

The data that supports the findings of this study are available in the supplementary material of this article.

References

[1] a) Y. He, Z. Huang, K. Wu, J. Ma, Y.-G. Zhou, Z. Yu, *Chem. Soc. Rev.* **2022**, *51*, 2759; b) T. Rogge, N. Kaplaneris, N. Chatani, J. Kim, S. Chang, B. Punji, L. L. Schafer, D. G. Musaev, J. Wencel-Delord, C. A. Roberts, R. Sarpong, Z. E. Wilson, M. A. Brimble, M. J. Johansson, L. Ackermann, *Nat. Rev. Methods Primers* **2021**, *1*, 43; c) J. F. Hartwig, M. Larsen, *ACS Cent. Sci.* **2016**, *2*, 281; d) W. R. Gutekunst, P. S. Baran, *Chem. Soc. Rev.* **2011**, *40*, 1976; e) L. McMurray, F. O'Hara, M. J. Gaunt, *Chem. Soc. Rev.* **2011**, *40*, 1885; f) H. M. L. Davies, D. Morton, *Chem. Soc. Rev.* **2011**, *40*, 1857; g) M. P. Doyle, R. Duffy, M. Ratnikov, L. Zhou, *Chem. Rev.* **2010**, *110*, 704.

[2] a) J. Martínez-Laguna, J. Altarejos, M. A. Fuentes, G. Sciortino, F. Maseras, J. Carreras, A. Caballero, P. J. Pérez, *J. Am. Chem. Soc.* **2024**, *146*, 34014; b) M. Álvarez, F. Molina, P. J. Pérez, *J. Am. Chem. Soc.* **2022**, *144*, 23275; c) L. Zhaohong, C. Shanshan, Y. Weijie, W. Jiayi, Y. Fanhua, A. A. Edward, X. Bi, *Chem* **2020**, *6*, 2110; d) K. Liao, Y.-F. Yang, Y. Li, J. N. Sanders, K. N. Houk, D. G. Mussaev, H. M. L. Davies, *Nat. Chem.* **2018**, *10*, 1048; e) L. Kuangbiao, N. Solymar, G. M. Djamaladdin, B. John, M. L. D. Huw, *Nature* **2016**, *533*, 230; f) K. Liao, T. C. Pickel, V. Botardkikh, J. Bacsa, D. G. Mussaev, H. M. L. Davies, *Nature* **2017**, *551*, 609; g) A. Caballero, E. Despagnet-Ayoub, M. M. Díaz-Requejo, A. Díaz-Rodríguez, M. E. González-Núñez, R. Mello, B. K. Muñoz, W.-S. Ojo, G. Asensio, M. Etienne, P. J. Pérez, *Science* **2011**, *332*, 835.

[3] a) B. M. Trost, A. S. K. Hashmi, *J. Am. Chem. Soc.* **1994**, *116*, 2183; b) B. M. Trost, A. S. K. Hashmi, *Angew. Chem. Int. Ed. Engl.* **1993**, *32*, 1085; c) J. F. Briones, H. M. L. Davies, *J. Am. Chem. Soc.* **2013**, *135*, 13314; d) X. Xu, P. Y. Zavalij, M. P. X. Doyle, *Angew. Chem. Int. Ed.* **2013**, *52*, 12664; e) Y. Qian, P. J. Zavalij,

W. Hu, M. P. Doyle, *Org. Lett.* **2013**, *15*, 1564; f) Q. Q. Cheng, J. Yedoyan, H. Arman, M. P. Doyle, *J. Am. Chem. Soc.* **2016**, *138*, 44; g) E. López, L. A. López, *Angew. Chem. Int. Ed.* **2017**, *56*, 5121; h) K. Dong, A. Humeidi, W. Griffith, H. Arman, X. Xu, M. P. Doyle, *Angew. Chem. Int. Ed.* **2021**, *60*, 13394.

[4] a) H. M. Davies, T. Clark, L. A. Church, *Tetrahedron Lett.* **1989**, *30*, 5057; b) H. M. L. Davies, E. Saikali, T. J. Clark, E. H. Chee, *Tetrahedron Lett.* **1990**, *31*, 6299; c) H. M. L. Davies, B. H. Hu, E. Saikali, P. R. Bruzinski, *J. Org. Chem.* **1994**, *59*, 4535.

[5] For a recent work, see:M. Bao, L. De Angelis, M. S. Rada, M. Baird, H. Arman, D. Wherritt, M. P. Doyle, *Chem Catal.* **2023**, *3*, 100778.

[6] For a comparison of the reactivity of metallocarbenes with different coinage metals, see:M. Besora, A. A. C. Braga, W. M. C. Sameera, J. Urbano, M. R. Fructos, P. J. Pérez, F. Maseras, *J. Organomet. Chem.* **2015**, *784*, 2.

[7] a) Y. Lian, H. M. L. Davies, *Org. Lett.* **2010**, *12*, 924; b) Y. Lian, H. M. L. Davies, *Org. Lett.* **2012**, *14*, 1934; c) D.-X. Zhu, H. Xia, J.-G. Liu, L. W. Chung, M.-H. Xu, *J. Am. Chem. Soc.* **2021**, *143*, 2608; d) T.-Y. Wang, X.-X. Chen, D.-X. Zhu, L. W. Chung, M.-H. Xu, *Angew. Chem. Int. Ed.* **2022**, *61*, e202207008.

[8] a) H. M. L. Davies, Y. Yokota, *Tetrahedron Lett.* **2000**, *41*, 4851; b) C. Qin, H. M. L. Davies, *Org. Lett.* **2013**, *15*, 6152; c) G. Xu, K. Liu, Z. Dai, J. Sun, *Org. Biomol. Chem.* **2017**, *15*, 2345; d) C. Zhang, H. Li, C. Pei, L. Qiu, W. Hu, X. Bao, X. Xu, *ACS Catal.* **2019**, *9*, 2440; e) W. Yang, M. Pu, X. Lin, M. Chen, Y. Song, X. Liu, Y.-D. Wu, X. Feng, *J. Am. Chem. Soc.* **2021**, *143*, 9648.

[9] P. García-Martínez, O. Bernardo, L. A. López, *Chem Catal.* **2023**, *3*, 100770.

[10] Y. Yang, Z. Liu, Q. Song, P. Sivaguru, G. Zanoni, K. Wang, Q. Bi, X. Bi, *Chem Catalysis* **2022**, *2*, 563.

[11] F. Miege, C. Meyer, J. Cossy, *Chem. Eur. J.* **2012**, *18*, 7810.

[12] a) P. Nösel, L. Nunes dos Santos Comprido, T. Lauterbach, M. Rudolph, F. Rominger, A. S. K. Hashmi, *J. Am. Chem. Soc.* **2013**, *135*, 15662; b) Z. Zheng, L. Zhang, *Org. Chem. Front.* **2015**, *2*, 1556.

[13] M. Mato, A. M. Echavarren, *Angew. Chem. Int. Ed.* **2018**, *58*, 2088.

[14] S. Peil, A. Gutiérrez González, M. Leutzsch, A. Fürstner, *J. Am. Chem. Soc.* **2022**, *144*, 4158.

[15] a) C. Pei, C. Zhang, Y. Qian, X. Xu, *Org. Biomol. Chem.* **2018**, *16*, 8677. b) Ò. Torres, A. Pla-Quintana, *Tetrahedron Lett.* **2016**, *57*, 3881.

[16] a) A. Padwa, T. J. Blacklock, R. Loza, *J. Am. Chem. Soc.* **1981**, *103*, 2404. b) A. Padwa, S. L. Xu, *J. Am. Chem. Soc.* **1992**, *114*, 5881.

[17] T. R. Hoye, C. J. Dinsmore, *J. Am. Chem. Soc.* **1991**, *113*, 4343.

[18] a) For examples from our group, see: Ò. Torres, T. Parella, M. Solà, A. Roglans, A. Pla-Quintana, *Chem. Eur. J.* **2015**, *21*, 16240; b) Ò. Torres, A. Roglans, A. Pla-Quintana, *Adv. Synth. Catal.* **2016**, *358*, 3512; c) Ò. Torres, M. Solà, A. Roglans, A. Pla-Quintana, *Chem. Commun.* **2017**, *53*, 9922; d) À. Díaz-Jiménez, R. Monreal-Corona, M. Solà, A. Poater, A. Roglans, A. Pla-Quintana, *ACS Catal.* **2024**, *14*, 7381.

[19] a) For selected examples, see: K. O. Marichev, H. Qiu, A. C. Offield, H. Arman, M. P. Doyle, *J. Org. Chem.* **2016**, *81*, 9235; b) Y. Zheng, M. Bao, R. Yao, L. Qiu, X. Xu, *Chem. Commun.* **2018**, *54*, 350; c) X. Wang, Y. Zhou, L. Qiu, R. Yao, Y. Zheng, C. Zhang, X. Bao, X. Xu, *Adv. Synth. Catal.* **2016**, *358*, 1571; d) S. Jansone-Popova, J. A. May, *J. Am. Chem. Soc.* **2012**, *134*, 17877; e) K. Dong, X. Fan, C. Pei, Y. Zheng, S. Chang, J. Cai, L. Qiu, Z.-X. Yu, X. Xu, *Nat. Commun.* **2020**, *11*, 2363; f) K. Hong, Y. Zhou, H. Yuan, Z. Zhang, J. Huang, S. Dong, W. Hu, Z.-X. Yu, X. Xu, *Nat. Commun.* **2023**, *14*, 6378.

[20] K. Dong, C. Pei, Q. Zeng, H. Wei, M. P. Doyle, X. Xu, *ACS Catal.* **2018**, *8*, 9543.

[21] À. Díaz-Jiménez, R. Monreal-Corona, A. Poater, M. Álvarez, E. Borrego, P. J. Pérez, A. Caballero, A. Roglans, A. Pla-Quintana, *Angew. Chem. Int. Ed.* **2023**, *62*, e202215163.

[22] J. M. Fukuto, F. R. Jensen, *Acc. Chem. Res.* **1983**, *16*, 177.

[23] R. Laplaza, M. D. Wodrich, C. Corminboeuf, *J. Phys. Chem. Lett.* **2024**, *15*, 7363.

[24] a) L. Falivene, Z. Cao, A. Petta, L. Serra, A. Poater, R. Oliva, V. Scarano, L. Cavallo, *Nat. Chem.* **2019**, *11*, 872; b) S. Escayola, N. Bahri-Laleh, A. Poater, *Chem. Soc. Rev.* **2024**, *53*, 853.

[25] J. M. Muñoz-Molina, T. R. Belderrain, P. J. Pérez, *Coord. Chem. Rev.* **2019**, *390*, 171.

[26] Y. Deng, L. A. Massey, P. Y. Zavalij, M. P. Doyle, *Angew. Chem. Int. Ed.* **2017**, *56*, 7479.

[27] a) A. M. Rodríguez, F. Molina, M. M. Díaz-Requejo, P. J. Pérez, *Adv. Synth. Catal.* **2020**, *362*, 1998; b) M. Álvarez, M. Besora, F. Molina, F. Maseras, T. R. Belderrain, P. J. Pérez, *J. Am. Chem. Soc.* **2021**, *143*, 4837; c) A. M. Rodríguez, J. Pérez-Ruiz, F. Molina, A. Poveda, R. Pérez-Soto, F. Maseras, M. M. Díaz-Requejo, P. J. Pérez, *J. Am. Chem. Soc.* **2022**, *144*, 10608; d) M. R. Rodríguez, A. M. Rodríguez, S. López-Resano, M. A. Pericàs, M. M. Díaz-Requejo, F. Maseras, P. J. Pérez, *ACS Catal.* **2023**, *13*, 706.

[28] We initially selected the $Tp(CF_3)_2$,^{Br} ligand for extending the study to copper. However, reactions with $Tp(CF_3)_2$,^{Br}Cu showed no conversion of the starting material. Computational analysis revealed an activation barrier of 24.6 kcal·mol^{-1} for the initial step (ligand dissociation and N_2 extrusion), compared to 20.9 kcal·mol^{-1} for Tp^{Br3}Cu. This 3.7 kcal·mol^{-1} increase likely accounts for the failure to generate the carbene intermediate under standard conditions.

[29] M. Álvarez, F. Villalba, M. Casciotti, F. Molina, G. Sciortino, A. Lledós, A. C. Albéniz, T. R. Belderrain, P. J. Pérez, *Chem* **2024**, *10*, 1576.

[30] a) S. E. Cleary, X. Li, L.-C. Yang, K. N. Houk, X. Hong, M. Brewer, *J. Am. Chem. Soc.* **2019**, *141*, 3558;

b) E. García-Padilla, I. Escofet, F. Maseras, A. M. Echavarren, *ChemPlusChem* **2024**, *89*, e202300502; c) Y.-B. Chen, L.-G. Liu, Z.-Q. Wang, R. C. Xin Lu, B. Zhou, L.-W. Ye, *Nat. Commun.* **2024**, *15*, 2232; d) Y.-X. Zheng, L.-G. Liu, T.-Q. Hu, X. Li, Z. Xu, X. Hong, X. Lu, B. Zhou, L.-W. Ye, *Nat Commun.* **2024**, *15*, 9227.

[31] R. Monreal-Corona, A. Pla-Quintana, A. Poater, *Trends Chem.* **2023**, *5*, 935.

[32] M. J. Frisch, G. W. Trucks, H. B. Schlegel, G. E. Scuseria, M. A. Robb, J. R. Cheeseman, G. Scalmani, V. Barone, G. A. Petersson, H. Nakatsuji, X. Li, M. Caricato, A. V. Marenich, J. Bloino, B. G. Janesko, R. Gomperts, B. Mennucci, H. P. Hratchian, J. V. Ortiz, A. F. Izmaylov, J. L. Sonnenberg, D. Williams-Young, F. Ding, F. Lipparini, F. Egidi, J. Goings, B. Peng, A. Petrone, T. Henderson, et al., *Gaussian 16, Revision A.03*, D. J. Gaussian, Inc., Wallingford CT **2016**.

[33] a) A. Becke, *Phys. Rev. A: At. Mol. Opt. Phys.* **1988**, *38*, 3098; b) J. P. Perdew, *Phys. Rev. B: Condens. Matter Mater. Phys.* **1986**, *33*, 8822; c) J. P. Perdew, *Phys. Rev. B: Condens. Matter Mater. Phys.* **1986**, *34*, 7406.

[34] S. Grimme, J. Antony, S. Ehrlich, H. Krieg, *J. Chem. Phys.* **2010**, *132*, 154104.

[35] S. Grimme, S. Ehrlich, L. Goerigk, *J. Comput. Chem.* **2011**, *32*, 1456.

[36] a) U. Haeusermann, M. Dolg, H. Stoll, H. Preuss, P. Schwerdtfeger, S. Pitzer, *Mol. Phys.* **1993**, *78*, 1211; b) W. Küchle, M. Dolg, H. Stoll, H. Preuss, *J. Chem. Phys.* **1994**, *100*, 7535; c) T. Leininger, A. Nicklass, H. Stoll, M. Dolg, P. Schwerdtfeger, *J. Chem. Phys.* **1996**, *105*, 1052.

[37] P. J. Hay, W. R. Wadt, *J. Chem. Phys.* **1985**, *82*, 299.

[38] A. Schäfer, H. Horn, R. Ahlrichs, *J. Chem. Phys.* **1992**, *97*, 2571.

[39] C. Gonzalez, H. B. Schlegel, *J. Chem. Phys.* **1989**, *90*, 2154.

[40] a) A. D. Becke, *J. Chem. Phys.* **1993**, *98*, 5648; b) A. D. Becke, *J. Chem. Phys.* **1993**, *98*, 5648.

[41] F. Weigend, R. Ahlrichs, *Phys. Chem. Chem. Phys.* **2005**, *7*, 3297.

[42] A. V. Marenich, C. J. Cramer, D. G. Truhlar, *J. Phys. Chem. B* **2009**, *113*, 6378.